

C. HSIEH
O. MOMTAHAN
A. KARBASCHI
A. ADIBI[✉]

A compact lensless and slitless volume holographic spectrometer for diffuse source spectroscopy

School of Electrical and Computer Engineering, Georgia Institute of Technology, Atlanta, GA 30332, USA

Received: 10 August 2007/Revised version: 20 November 2007
Published online: 20 February 2008 • © Springer-Verlag 2008

ABSTRACT We present a simple, very compact, and inexpensive spectrometer for diffuse source spectroscopy using only a volume hologram (recorded by two spherical beams) and a CCD camera (or a detector array). We show that this spectrometer can operate well under spatially incoherent light illumination. We also show that the resolution of this spectrometer can be optimized by proper selection of the location of the CCD camera (or the detector array). The results show the possibility of using optimized holographic optical elements as the integrated collimating, dispersive, and light-collective components of spectrometers.

PACS 42.40.Pa; 42.79.-e

1 Introduction

Compact, portable, efficient, and low-cost spectrometers are of high interest in biological and environmental sensing. A conventional spectrometer consists of four major parts: a collimator, a wavelength-dispersive medium, a collector, and a detector. In conventional spectrometers, gratings are commonly used as wavelength-dispersive media and can separate wavelength channels of a spatially coherent incident beam very well. However, a spatially incoherent beam consisting of multiple spatial modes results in the spatial overlap of multiple wavelength channels in the output plane of the grating. To avoid this problem, a collimator which is composed of a narrow slit and a lens (or a concave mirror) is placed in front of the grating. The main drawback of this arrangement is the low throughput as the slit blocks most of the input power. Increasing the slit width to improve the throughput results in less resolution. This trade-off between resolution and throughput is another disadvantage of

a conventional spectrometer. Furthermore, the system requires good alignment to avoid extra loss of power.

We recently demonstrated a compact slitless holographic spectrometer [1] where we integrated the collimator (the slit and lens) and the grating into a spherical beam volume hologram (SBVH) recorded by the interference of a plane wave (i.e. reference beam) and a spherical beam (i.e. signal beam). When the SBVH is read by a plane wave from the direction of the recording spherical beam, the diffracted beam has a crescent shape due to partial Bragg matching [2, 3]. The position of the crescent at the back face of the volume hologram depends both on the reading wavelength and on the direction of the reading plane wave. This effect results in considerable crosstalk between different incident wavelength channels when the reading beam is a diffuse optical signal (i.e. it can be decomposed into several plane waves at different incident angles) with multiple wavelengths. To solve this ambiguity, a Fourier-

transform lens (that plays the same role as the collector in conventional spectrometers) is required behind the hologram, so that all diffracted crescents corresponding to different incident angles at the same incident wavelength overlap at the same location in the Fourier plane [4]. Therefore, the position of the Fourier spectrum of the crescents depends only on the incident wavelength, which is highly desirable for diffuse source spectroscopy.

In the holographic spectrometers that rely on only a single SBVH, the resolution throughput trade-off is similar to that in conventional spectrometers. For example, using a thicker volume hologram (i.e. larger L in Fig. 1a) results in better resolution (i.e. a thinner crescent) due to the sharper Bragg selectivity of the volume hologram. At the same time, the thinner crescent results in smaller output power, which reduces the throughput. This is similar to using a narrow slit in conventional spectrometers. However, several SBVHs can be multiplexed in the thicker material (due to the larger dynamic range) to encode each input wavelength channel into a series of narrow output crescents (i.e. using a more sophisticated spatial-spectral mapping). This enables multimodal multiplex spectroscopy [5, 6] that was recently implemented for throughput improvement in spectrometers. Thus, using thicker holographic materials with the holographic multiplexing technique results in better resolution without sacrificing the throughput.

One advantage of this slitless holographic spectrometer is that the diffuse source can be placed right in front of the SBVH without any input coupling,

✉ Fax: +1-404-894-4641, E-mail: adibi@ece.gatech.edu

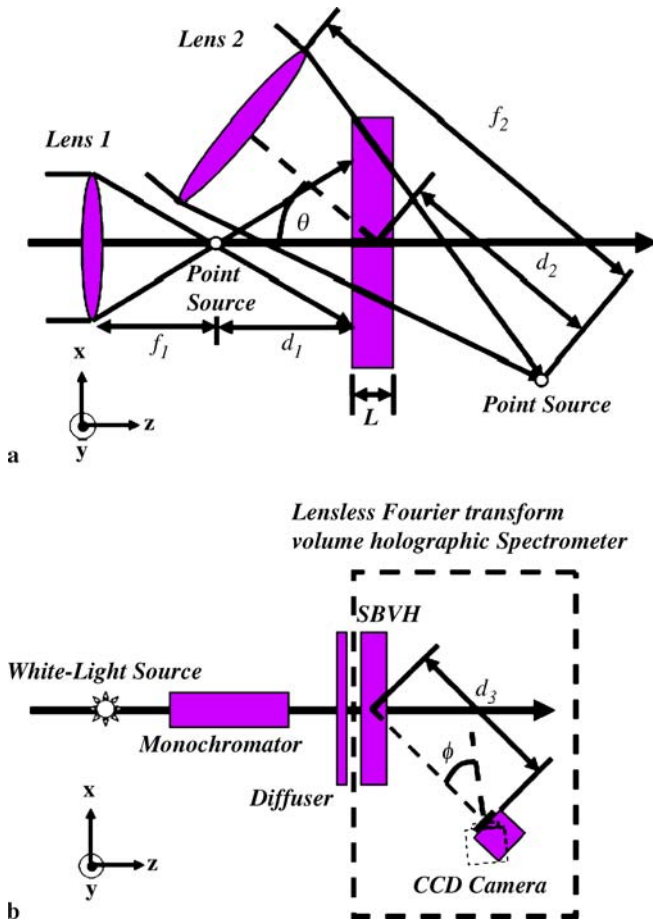


FIGURE 1 The schematics of (a) recording and (b) reading setups for a lensless volume holographic spectrometer. The recording material is a sample of Aprilis photopolymer with thickness $L = 300 \mu\text{m}$. The size of the hologram is 0.49 cm^2 . The diverging spherical beam is formed by focusing a plane wave in front of the recording medium with a lens with focal length $f_1 = 4.0 \text{ cm}$ and numerical aperture (NA) of 0.25 (corresponding to about 29° acceptance angle for the spectrometer in (b)). The distance between the recording medium and the focal point is $d_1 = 4.0 \text{ cm}$. The converging spherical beam is formed by focusing a plane wave behind the recording medium with a lens with focal length $f_2 = 6.5 \text{ cm}$ and numerical aperture (NA) of 0.25. The distance between the recording medium and the focal point is $d_2 = 4.0 \text{ cm}$. The angle between the direction of the converging spherical beam and the normal to the medium is $\theta = 35.64^\circ$. The distance between the CCD camera and the hologram in (b) is d_3 , and the angle between the direction of the diffracted beam and the normal to the CCD camera is φ . Both d_3 and φ are tunable for the calibration of this spectrometer

which reduces the alignment requirements. Besides, since no slit or lens is required in front of the hologram, this holographic spectrometer is more compact than the conventional one. However, the Fourier-transform lens behind the hologram is still essential for the slitless holographic spectrometer.

2 Demonstration of lensless spectrometer

To make the system more compact, we present here a new lensless volume holographic spectrometer. We show that the Fourier-transform lens can be further integrated into the SBVH as a holographic lens [7] and, therefore, the actual Fourier-transform lens

can be eliminated. To realize the holographic lens, the plane-wave reference in the original SBVH [1] is substituted with a converging spherical beam. Figure 1a shows the experimental setup for recording such SBVHs by use of two diverging and converging spherical beams. The converging recording beam (instead of a plane wave in the original demonstration of the slitless holographic spectrometer [1]) is used to add a quadratic phase term to the diffracted signal for performing Fourier transformation without an external lens. Figure 1b shows a general reading setup used for all the measurements in this paper. The hologram is read from the direction of the diverging recording spherical beam and the diffracted beam is in

the direction of the converging recording spherical beam. Assuming that read out is performed at the recording wavelength, the Fourier transform of the diffracted beam pattern (i.e. the crescent) is obtained at the focus of the reference beam, where the CCD camera is placed to capture the output signal. Since no lens or any optical device other than a volume hologram and a CCD camera is required, this spectrometer is more compact, less costly, less sensitive to input coupling alignment, and potentially more efficient compared to conventional spectrometers.

The hologram used in this paper is a SBVH recorded at $\lambda = 532 \text{ nm}$ in a $300\text{-}\mu\text{m}$ -thick sample of Aprilis photopolymer [8] using the setup shown in Fig. 1a with $f_1 = d_1 = d_2 = 4.0 \text{ cm}$ and $f_2 = 6.5 \text{ cm}$. More details of the experimental parameters are specified in the caption of Fig. 1. This SBVH is first read by a monochromatic collimated beam at $\lambda = 532 \text{ nm}$ obtained by passing white light through the monochromator as shown in Fig. 1b without the presence of the diffuser. The CCD camera (with 765×510 pixels and a pixel size of $9 \mu\text{m} \times 9 \mu\text{m}$) is located at $d_3 = 4.0 \text{ cm}$ (i.e. at the Fourier plane) and is perpendicular to the diffracted beam (i.e. $\varphi = 0^\circ$) in this case. The diffracted beam both at the output face of the hologram and on the CCD camera has a crescent shape [3] as shown in Fig. 2a. When the hologram is read by a monochromatic diffuse beam at $\lambda = 532 \text{ nm}$ with the presence of the rotating diffuser in Fig. 1b, the diffracted pattern at the output face of the hologram is diffuse light consisting of many overlapping crescents as shown in Fig. 2b. However, the diffracted beam pattern on the CCD camera has the crescent shape shown in Fig. 2c, which is similar to that shown in Fig. 2a except at the edge [3]. It is clear that the location of the diffracted crescent at the CCD camera plane is independent of the reading incident angle (since only one crescent is obtained on the CCD camera). Moreover, the position of the crescent on the CCD camera depends only on the incident wavelength of the diffuse reading beam. Thus, this simple system acts similarly to the slitless holographic spectrometer reported in [1] without any Fourier-transforming lens required.

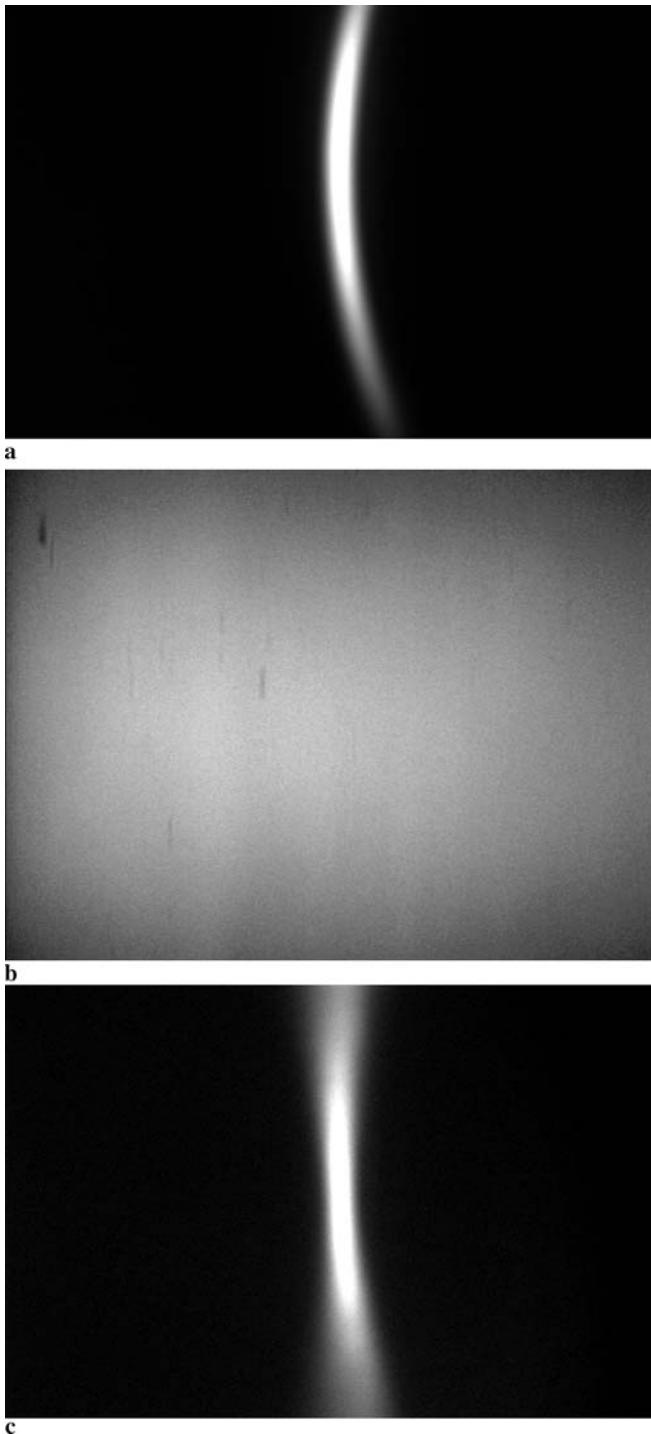


FIGURE 2 Diffracted patterns measured (a) at the focal point of the recording converging spherical beam when read by a collimated monochromatic beam ($\lambda = 532$ nm), (b) at the back face of the spherical beam volume hologram when read by a diffuse monochromatic beam ($\lambda = 532$ nm), and (c) at the focal point of the recording converging spherical beam when read by a diffuse monochromatic beam ($\lambda = 532$ nm). The hologram was recorded using the setup in Fig. 1a

3 System evaluation

Assuming that the paraxial approximation is applicable (i.e. first-order approximation), it is shown that the longitudinal magnification ratio of a holographic imaging system scales by

the ratio of the recording wavelength to the reading wavelength [9], which is not the case in refractive imaging (i.e. imaging with a lens). Therefore, it is expected that the Fourier transform of the diffuse crescents at the output of the hologram is produced at different dis-

tances from the hologram for different reading wavelengths. At larger numerical apertures, the diffracted beam at a shifted wavelength will no longer be a perfect spherical beam [9]. This causes aberration that can degrade the resolution of the spectrometer. To investigate these effects, we changed the reading wavelength to $\lambda = 590$ nm (which is far enough from the recording wavelength $\lambda = 532$ nm) and repeated the experiment using the setup in Fig. 1b with $d_3 = 4.0$ cm and $\varphi = 0^\circ$. The SBVH is first read without the presence of the diffuser. The diffracted beam pattern on the CCD camera has a crescent shape (shown in Fig. 3a) located at a different position compared to that in Fig. 2a (obtained at the reading wavelength of $\lambda = 532$ nm). This clear crescent shape of the diffracted beam is always obtained within the wavelength-detecting range (~ 100 nm) for this specific hologram of the spectrometer. However, the diffracted beam pattern at the CCD camera becomes blurred after adding a rotating diffuser in front of the hologram, as shown in Fig. 3b. By changing the position of the CCD camera along the direction of the diffracted beam to $d_3 = 3.4$ cm, we can find the correct position of the Fourier plane corresponding to $\lambda = 590$ nm and the clear crescent shape of the diffracted beam pattern is retrieved, as shown in Fig. 3c. It is inferred from Fig. 3 that the position of the Fourier plane changes with the incident wavelength and further optimization of the spectrometer is necessary to obtain the best resolution (i.e. smallest width of the crescent) for all wavelengths within the detection range.

To measure the wavelength dependence of the position of the Fourier plane of the SBVH (which is required for the optimization of the lensless spectrometer), we read the SBVH by monochromatic diffuse light using the experimental setup in Fig. 1b with $\varphi = 0^\circ$. For each reading wavelength, we moved the CCD camera along the direction of the diffracted beam and measured the full width at half maximum (FWHM) of the diffracted beam pattern (crescent) on the CCD camera at each position. Figure 4a shows the variation of the FWHM of the crescent with the CCD camera position (i.e. d_3 in Fig. 1b) for different wavelengths in the range of 442 nm to 552 nm. For each

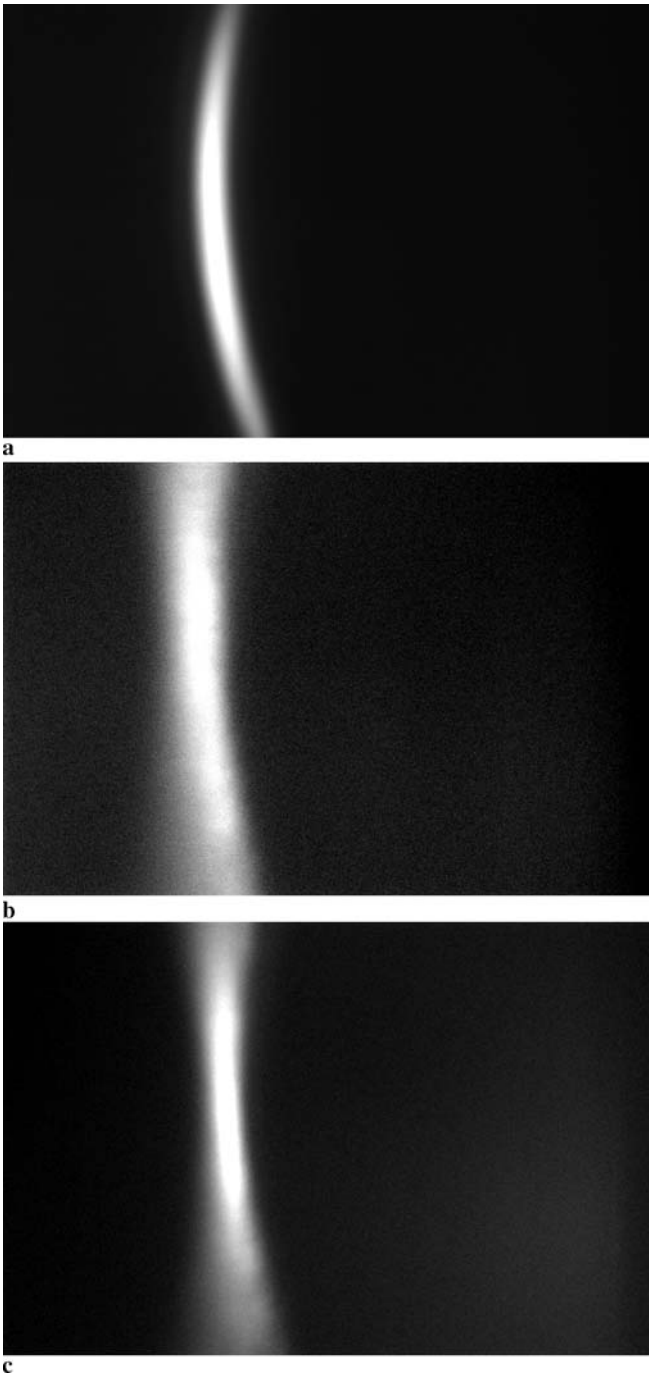


FIGURE 3 Diffracted patterns measured (using the setup in Fig. 1b) at the focal point of the recording converging spherical beam when read at $\lambda = 590$ nm by (a) a collimated monochromatic beam with CCD camera at $d_3 = 4.0$ cm, (b) a diffuse monochromatic beam with CCD camera at $d_3 = 4.0$ cm, and (c) a diffuse monochromatic beam with CCD camera at $d_3 = 3.4$ cm. The hologram was recorded using the setup in Fig. 1a with recording wavelength of $\lambda = 532$ nm

wavelength, the CCD camera position corresponding to the crescent with the minimum FWHM is the position of the optimal Fourier plane. Based on the data in Fig. 4a, the variation of the position of the Fourier plane (i.e. the location of the minimum FWHM of the crescent in Fig. 4a) with the incident wavelength is shown in Fig. 4b. The error bars shown

in Fig. 4b represent the range of the position of the Fourier plane with less than 10% broadening of the minimum FWHM of the crescent. The variation of the position of the optimal Fourier plane with wavelength (i.e. the solid curve in Fig. 4b) can be approximated by a linear function (i.e. the dashed line in Fig. 4b) with minimum error (less than 5%)

in the entire wavelength range. Thus, the optimal CCD camera positions for all wavelengths can be satisfied with a small error by carefully adjusting the tilt angle (φ) of the CCD camera according to the slope of the dashed line in Fig. 4b.

4 System calibration

To demonstrate the effect of the incident wavelength on the resolution of the proposed lensless spectrometer, we used the experimental setup in Fig. 1b (with the monochromator and the rotating diffuser present) with the CCD camera tilted by $\varphi = 50^\circ$ and scanned the input wavelength from $\lambda = 482$ nm to $\lambda = 582$ nm with 5-nm spacing, which is controlled by the monochromator with full width at half maximum (FWHM) resolution equal to 8 nm. The light intensity at all points in the output plane for each incident wavelength is captured using the CCD camera. Note that the optimal tilt angle calculated using the results in Fig. 4b is $\varphi = 79^\circ$. However, due to the properties of our CCD camera and the setup in Fig. 1b, we used $\varphi = 50^\circ$, which is not too far from optimum. The normalized output intensity (i.e. the output intensity divided by the input intensity) with respect to the location in the horizontal axis on the CCD camera is shown in Fig. 5. Each curve in Fig. 5 corresponds to one incident wavelength. Figure 5 clearly shows that the output spatial intensity pattern is a function of the incident wavelength under spatially incoherent light illumination. Note that the peak of the normalized intensity is different for different wavelengths because the efficiency of partial Bragg matching from the SBVH depends on the wavelength. These curves can be made more similar by optimizing the recorded hologram, and such optimization is currently being studied. Nevertheless, Fig. 5 shows that: (1) the proposed lensless spectrometer is capable of separating wavelength channels of a diffuse input signal without requiring a Fourier-transforming lens and (2) by tilting the CCD camera appropriately, the dependence of the resolution on the incident wavelength (i.e. the widths of the peak at different wavelengths) can be minimized. The operation spectrum range, which depends on the properties

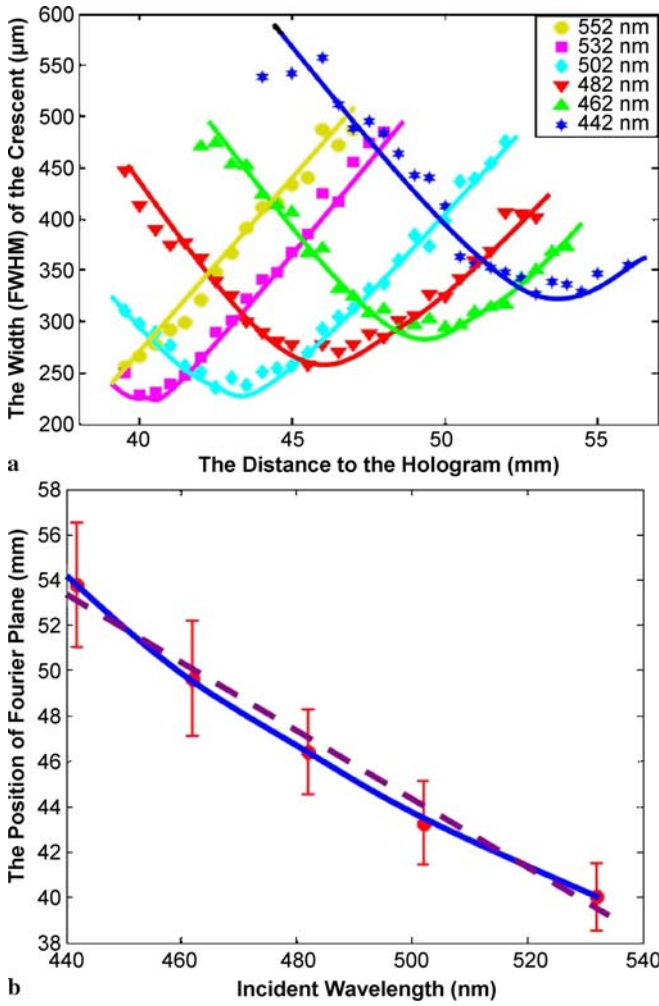


FIGURE 4 (a) The effect of the incident wavelength on the position of the Fourier plane and the full width at half maximum (FWHM) of the diffracted beam pattern (crescent) in the lensless spectrometer. Each curve represents the variation of the FWHM of the crescent at the CCD camera plane with the position of the CCD camera (d_3 in Fig. 1b) at a single wavelength. (b) The variation of the optimal position of the CCD camera (i.e. the Fourier plane) with the incident wavelength in the lensless spectrometer. Error bars show the spatial range for which the FWHM of the crescent on the CCD camera differs from the minimum value by less than 10%

of the recording material and the recording beams, can be further extended by changing the design parameters such as the divergence angle of the recording spherical wave. Further increase in this range can be achieved by simply rotating the SBVH.

For the lensless spectrometer demonstrated in Fig. 5, the overall efficiency (i.e. the diffracted power in a crescent divided by the total incident power) depends on the spatial profile of the incident beam (including the degree of spatial coherence). In the worst-case scenario (i.e. a fully diffuse incident beam), this value is in the range of 1%, which is similar to (if not better than) that in conventional spectrometers. The efficiency can be further improved by

multiplexing a few holograms to encode each input wavelength channel into a series of output crescents, as mentioned earlier. Moreover, the acceptance angle of this lensless holographic spectrometer is limited by the numerical aperture (NA) of the recording lens that was used to generate the diverging spherical beam (i.e. the lens 1 shown in Fig. 1a). Based on the theoretical model developed in [3, 4], the hologram recorded by a certain diverging angle of the recording spherical beam allows the same range of reading spatial modes (i.e. the acceptance angles) to be partially Bragg matched. Thus, the acceptance angle of the holographic spectrometer can be improved by using a larger diverging angle for the recording spherical beam

by using a recording lens with a higher NA. For recording the hologram used in this paper, we use a recording lens with NA = 0.25. Thus, the acceptance angle of the resulting spectrometer is 29°.

Generally, recording the interference pattern of spherical beams made by regular lenses is the simplest method for realization of a holographic lens. In fact, there are a few effects that can potentially degrade the quality of a holographic lens versus a similar normal refractive lens in terms of the aberration and wavelength dependence (i.e. dispersion). To evaluate these effects on the lensless spectrometer, we define a resolution deterioration rate (R_D) as

$$R_D = \frac{|R_{\lambda_c} - R_{\lambda_e}|}{R_{\lambda_c}} \frac{1}{|\lambda_c - \lambda_e|} \quad (\text{nm}^{-1}), \quad (1)$$

where R_{λ_c} is the resolution for the central region of the full operating wavelength range and R_{λ_e} is the resolution for the edge region of the full operating wavelength range. The resolution R_λ is determined by

$$R_\lambda = \frac{w_{\text{FWHM}}(\lambda)}{\Delta x_{\text{peak}}(\lambda)/\Delta\lambda} \quad (\text{nm}), \quad (2)$$

where $w_{\text{FWHM}}(\lambda)$ is the FWHM of the crescent for one specific wavelength and $\Delta x_{\text{peak}}(\lambda)/\Delta\lambda$ is the movement of the center of the crescent with respect to the change of the incident wavelength. The resolution defined in this paper is the same as that used in commercial spectrometers. Both $w_{\text{FWHM}}(\lambda)$ and $\Delta x_{\text{peak}}(\lambda)/\Delta\lambda$ can be obtained from Fig. 5, and the resolution deterioration rate (R_D) is 0.00289 nm⁻¹, which can be calculated by using (1) and (2). By comparing the resolution deterioration rates between the lensless spectrometer and the conventional slitless holographic spectrometer [1] (which incorporates a Fourier-transforming lens), we found that the former is only 2.5% larger (i.e. worse) than the latter. Thus, a competitive performance can still be achieved by integrating the lens function (i.e. quadratic phase term) into the SBVH in the lensless spectrometer proposed in this paper, even if a holographic lens can not perform perfectly as a normal refractive lens in many aspects. In fact, since this hologram primarily performs Fourier transformation for the spatial-spectral mapping but not the imaging,

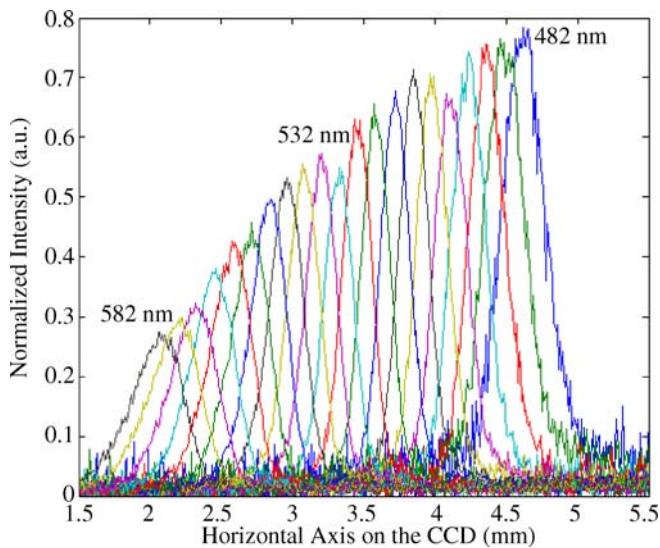


FIGURE 5 Normalized intensity versus the location along the horizontal axis on the CCD camera with $\varphi = 50^\circ$ and $d_3 = 4.0$ cm in Fig. 1b. The hologram is read by diffuse light (using the rotating diffuser) with single wavelength at each time. The hologram was recorded using the setup in Fig. 1a

some of the imperfections can be tolerated as they actually appear as part of the spatial–spectral mapping, which will be automatically taken into account during the spectrometer calibrations.

With the data provided, we have shown that the lensless spectrometer performs as well as the slitless holographic spectrometer with the external lens. Furthermore, the lensless spectrometer as a holographic diffractive element (HOE) offers the potential of eliminating all of the imperfections at almost no cost per each recorded HOE. In fact, with a more sophisticated recording configuration (e.g. exploiting computer-generated holograms as pre-distorting elements [10] or by using an optimally designed diffractive optical element instead of two spherical beams to record the hologram [11]), it is shown that the aberration of the thin holographic lenses can be minimized. Since the effect of the Bragg selectivity of the volume hologram is equivalent to filtering a range of the diffracted plane wave components [3,4] (i.e. deleting several plane waves propagating in non-Bragg-matched directions and diffract-

ing only the ones in a narrow range of spatial frequencies), a similar procedure as in [11] can be used to minimize the effect of aberrations for the volume holograms used in lensless spectrometers. Moreover, it facilitates designing dispersive elements having more spatial–spectral diversity to improve the resolution and/or the throughput.

It should also be noted that the properties of the lensless spectrometer are mainly obtained from the phase distribution of the recorded volume hologram. The small spatial variations of the diffraction efficiency of the hologram have minimal effect on the results. However, these variations can be compensated during the recording to obtain a hologram with uniform diffraction efficiency.

5 Conclusion

In conclusion, we successfully demonstrated a lensless spectrometer for diffuse source spectroscopy using a SBVH recorded by one converging spherical beam and one diverging spherical beam. In particular,

we showed that all the optical components of the conventional spectrometer can be implemented in a single volume hologram that is designed properly for the spectrometer. We also showed that the resolution of the spectrometer at different wavelengths is similar by choosing the tilt angle of the CCD camera appropriately. Since only a hologram and a CCD camera are required for this spectrometer, it can be made very compact and inexpensive with less alignment sensitivity compared to the conventional spectrometers. Finally, since any complex hologram with desired properties can be recorded without adding complexity to the spectrometer (i.e. a hologram and a CCD camera), this lensless spectrometer can be used for designing special purpose spectrometers with considerable design flexibility.

ACKNOWLEDGEMENTS This work was supported by the National Institute on Alcohol Abuse and Alcoholism through the Integrated Alcohol Sensing and Data Analysis program under Contract No. N01-AA-23013 and by the David and Lucile Packard Foundation. The authors thank D.J. Brady for useful discussions.

REFERENCES

- 1 C. Hsieh, O. Momtahan, A. Karbaschi, A. Adibi, *Opt. Lett.* **30**, 836 (2005)
- 2 A. Karbaschi, C. Hsieh, O. Momtahan, A. Adibi, M.E. Sullivan, D.J. Brady, *Opt. Express* **12**, 3018 (2004)
- 3 O. Momtahan, C. Hsieh, A. Karbaschi, A. Adibi, M.E. Sullivan, D.J. Brady, *Appl. Opt.* **43**, 6557 (2004)
- 4 O. Momtahan, C. Hsieh, A. Adibi, D. Brady, *Appl. Opt.* **45**, 2955 (2006)
- 5 Z. Xu, Z. Wang, M.E. Sullivan, D.J. Brady, S.H. Foulger, A. Adibi, *Opt. Express* **11**, 2126 (2003)
- 6 S.D. Feller, H. Chen, M.E. Gehm, D.J. Brady, C. Hsieh, O. Momtahan, A. Adibi, *Opt. Express* **15**, 5625 (2007)
- 7 A.K. Richter, F.P. Carlson, *Appl. Opt.* **13**, 2924 (1974)
- 8 H.J. Coufal, D. Psaltis, G.T. Sincerbox (eds.), *Holographic Data Storage* (Springer, New York, 2000)
- 9 R.W. Meier, *J. Opt. Soc. Am.* **55**, 987 (1965)
- 10 K. Winick, *J. Opt. Soc. Am.* **72**, 143 (1982)
- 11 S. Kirkpatrick, C.D. Gelatt, M.P. Vecchi, *Science* **220**, 671 (1983)